A Centralized Energy Management System for Isolated Microgrids

Daniel E. Olivares, *Student Member, IEEE*, Claudio A. Cañizares, *Fellow, IEEE* and Mehrdad Kazerani, *Senior Member, IEEE*

***Abstract*—This paper presents the mathematical formulation of the microgrid's energy management problem and its implementation in a centralized Energy Management System (EMS) for isolated microgrids. Using the model predictive control technique, the optimal operation of the microgrid is determined using an extended horizon of evaluation and recourse, which allows a proper dispatch of the energy storage units. The energy management problem is decomposed into Unit Commitment (UC) and Optimal Power Flow (OPF) problems in order to avoid a mixed-integer non-linear formulation. The microgrid is modelled as a three-phase unbalanced system with presence of both dispatchable and non-dispatchable distributed generation. The proposed EMS is tested in an isolated microgrid based on a CIGRE medium-voltage benchmark system. Results justify the need for detailed three-phase models of the microgrid in order to properly account for voltage limits and procure reactive power support.**

***Index Terms*—Microgrid, smart grid, energy management system, model predictive control, optimal dispatch, OPF.**

NOMENCLATURE

Parameters

Δt_{k_t}	Absolute time between step k_t and step k_t+1
$\eta_{g_b}^{in}$,$\eta_{g_b}^{out}$	Battery-ESS charge & discharge efficiencies, %
η_{el}, η_{fc}	Electrolizer & Fuel-cell efficiencies (HHV), %
A, B, C, D	Three-phase ABCD parameter matrices, p.u.
a_g	Quadratic term factor of cost function of generating units
b_g	Linear term factor of cost function of generating units
c_g	Constant term of cost function of generating units
$C_{sdn,g}$	Shut-down cost generating units
$C_{sup,g}$	Start-up cost generating units
HHV	Hydrogen Higher Heating Value, kWh/Nm^3
K_{loss}	Constant active power losses of connection interface
M_{dn}	Minimum time down of generating units
M_{up}	Minimum time up of generating units
$P_{p,L}$	Active power of loads per phase, p.u.
$Q_{p,L}$	Reactive power of loads per phase, p.u.
R_{dn}	Maximum ramp-down of generating units
r_{loss}	Series resistance of connection interface
R_{up}	Maximum ramp-up of generating units
t_{k_t}	Absolute time at time-step k_t
x''_d, x''_q	Unsaturated direct- and quadrature-axis subtransient reactances of synchronous generator
x_d	Direct-axis synchronous reactance of synchronous generator
x_{pos}, x_{neg}, x_0	Positive, negative and zero sequence reactances of synchronous generator
$Z_{p,L}$	Load impedance per phase, p.u.
$\mathbf{0}$	3-by-3 zero matrix
$\mathbf{A}$	3-by-3 sequence conversion matrix
$\mathbf{I}$	3-by-3 identity matrix

Indices

g	Generating units
g_b	Battery banks
g_d	Dispatchable generators
g_i	Induction generators
g_n	Generating units connected to node n
g_s	Synchronous generators
g_{fc}, g_{el}	Fuel-cells and electrolizers
H_{tank}	Hydrogen tanks
k_t	Time-steps
L	Index for loads, L = 1,...NL
l	Index for series elements, l=1,...Nl
L_n	Loads connected to node n
p	Index for phases, $p = a, b, c$
r	Index for receiving-end
r_n	Receiving-ends connected to node n
s	Index for sending-end
s_n	Sending-ends connected to node n

Variables

u_g	Start-up decision variable
v_g	Shut-down decision variable
w_g	Unit-commitment decision variable
$\overline{E}$	Vector of steady-state internal voltage phasors of synchronous generators, p.u.
$\overline{I}$	Vector of three-phase line current phasors, p.u.
$\overline{V}$	Vector of three-phase line voltage phasors, p.u.
I_p	Line current phasor, p.u.
$I_{p,p}$	Line-to-line current phasor, p.u.
$P_{g_b}^{in}$	Battery–ESS input power
$P_{g_b}^{out}$	Battery–ESS output power
P_{loss}	Total active power losses of connection interface
$P_{p,g}$	Active power of generating units per phase, p.u.
P_{source}	Total active power produced by the generating unit
$Q_{p,g}$	Reactive power of generating units per phase, p.u.
SOC	State of charge of an ESS
V_p	Line voltage phasor, p.u.
$V_{p,p}$	Line-to-line voltage phasor, p.u.

This work has been partially supported by an NSERC Discovery grant.

The authors are with the Department of Electrical and Computer Engineering, University of Waterloo, Waterloo, ON N2L 3G1, Canada. Email: dolivare@uwaterloo.ca, ccanizares@uwaterloo.ca, mkazeran@ecemail.uwaterloo.ca

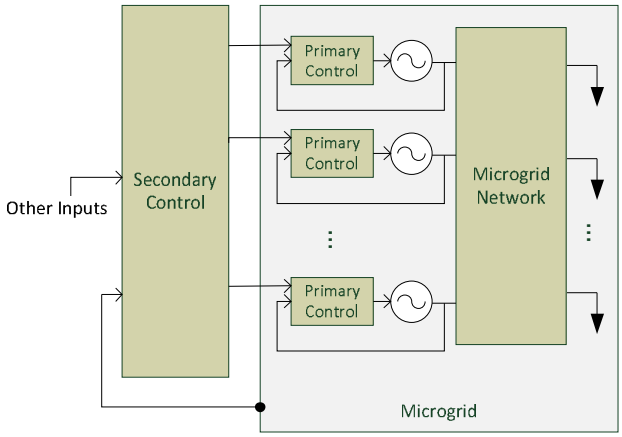

Fig. 1: Primary and secondary control levels in an isolated microgrid.

I. Introduction

THE concept of microgrid, defined and discussed in [1] and [2], has drawn considerable attention from researchers over the last decade, given its potential to achieve a reliable and efficient integration of Distributed Energy Resources (DER) in today's power systems. Several definitions have been proposed for a microgrid, but, in general, microgrids can be defined as a cluster of loads and DER units that are operated in coordination and perceived as a single element by the main grid. Two modes of operation can be identified for a microgrid: grid-connected and stand-alone.

Given the different control tasks and time constants involved in the operation of a microgrid, a hierarchical approach has been adopted for designing microgrids' control systems. In this work, following a structure similar to the one proposed in [3], three control levels are identified: primary, secondary, and tertiary control. Primary control relies exclusively on local measurements, and is composed of an output control stage responsible for tracking voltage and current references, and a power sharing control responsible for the adequate share of real and reactive power mismatches. Secondary control, also known as Energy Management System (EMS), is responsible for the reliable and economical operation of the microgrid, and is the highest hierarchical level in control of isolated microgrids. Primary and secondary control levels are illustrated in Fig. 1 for an isolated microgrid. Tertiary control is responsible for the coordinated operation of multiple microgrids and the host grid. This paper concentrates on the development of an EMS for real-time autonomous applications in isolated microgrids.

Two main approaches can be identified in the secondary control: centralized and decentralized. The decentralized approach aims to achieve economical operation of a microgrid while providing the highest possible autonomy to the different DERs and loads. Decentralized approaches have been primarily addressed in the technical literature by using the Multi-Agent Systems (MAS) framework [4]–[6]. The centralized approach features a central controller that is provided with the relevant information about the microgrid, as well as the information from forecasting systems, in order to determine the dispatch of the resources according to the selected objectives [7]–[11]. In [12], two options are identified for the algorithms in a centralized approach, namely, real-time optimization and expert systems.

In stand-alone microgrids, which is the focus of this paper, a high level of coordination is required among the DER units participating in control tasks, which makes the centralized approach the most suitable for this application [7]. Previous works on centralized EMS approaches have focused on the development of mathematical models of the microgrid's operation and components with emphasis on Mixed-Integer Linear Programming (MILP) formulations [8]–[10], most of which present little or no representation of the distribution system. Technical literature on energy management in the context of active distribution system has recognized the need for a detailed modelling of the system to properly manage reactive power requirements and account for non-negligible system losses [13], [14]; however, modelling the distribution system typically introduces non-linear equations that increase the complexity of the formulation and increase the computational times to obtain the solution. System unbalance may have an important effect on the optimal operation of distribution systems [15]; however, this condition has not been properly modelled in the context of EMSs for microgrids.

This paper presents the control architecture and mathematical models of a novel, autonomous, centralized EMS for stand-alone microgrids that features a detailed three-phase (unbalanced) model of the system. A decomposition approach allows the proposed EMS to be solved within the desired time-window to make it suitable for real-time applications, which is demonstrated in a realistic isolated microgrid test-system. The main contribution of this work are:

- A novel, highly detailed, mathematical formulation of the energy management problem for remote, isolated microgrids is presented, which is able to account for the effects of power flow constraints and system unbalances on the optimal operation of a microgrid.
- A problem decomposition approach is proposed that allows the high-detail model to be solved in suitable computational times for real-time applications, including new heuristics to correct infeasible dispatch solutions due to unmet reactive power requirements.
- The advantages of the proposed approach are discussed and compared with a classical balanced approximation of the microgrid, showing the potential problems of neglecting the effect of system unbalances.

The rest of the paper is organized as follows: Section II presents the formulation of the energy management problem, and the mathematical models of the microgrid's components and operation. Section III discusses the architecture and framework of the proposed EMS. Section IV describes the microgrid used for testing and validation of the proposed EMS, presenting and discussing various relevant results. Finally, the main contributions of the presented work are highlighted in Section IV.

II. Mathematical Energy Management Model

In microgrids with centralized EMS, the dispatch of available resources is the result of solving a mathematical programming problem. The formulation of the energy management problem includes constraints associated with operational limits of the generating units, power flow/power balance, energy balance of Energy Storage Systems (ESSs), system operator settings, and spinning reserve.

In addition to the time coupling introduced by constraints such as ramping-rates, minimum-up/minimum-down times, and start-up/shut-down times, in microgrids with significant shares of energy storage capacity and intermittent non-dispatchable energy resources, a stronger coupling exists in the operating conditions at different times. Additionally, the high operational flexibility of small generation units in terms of ramping-rates, minimum-up/minimum-down times, and start-up/shut-down times allow the unit-commitment decision variables to be determined with higher update rates as compared to bulk power systems. These particular characteristics require the energy management problem to be formulated as a multi-stage programming problem.

In general, the steady-state energy management problem to be solved in order to determine the best possible dispatch at time t with the available information can be written as follows:

$$\begin{aligned} \min_{u} \quad & \sum_{k_t=t}^{t+K} F(x_{k_t}, z_{k_t}, u_{k_t}, p_{k_t}) \\ \text{s.t.} \quad & z_{k_t+1} = m(x_{k_t}, z_{k_t}, u_{k_t}, p_{k_t}) \quad k_t = t, \ldots, t+K. \\ & g(x_{k_t}, z_{k_t}, u_{k_t}, p_{k_t}) = 0 \quad k_t = t, \ldots, t+K. \\ & h(x_{k_t}, z_{k_t}, u_{k_t}, p_{k_t}) \leq 0 \quad k_t = t, \ldots, t+K. \\ & \parallel u_{k_t+1} - u_{k_t} \parallel \leq \Delta u_{k_t}^{max} \quad k_t = t, \ldots, t+K. \end{aligned} \tag{1}$$

where $z_{k_t} \in R^w$ is a vector of discrete time-dependent variables, such as the state of charge of ESSs, and $p_{k_t} \in R^l$ is the vector of parameters representing the best available estimation at step $k_t = t$ of system demand, intermittent generation, fuel prices, etc., for all the time-steps in the multi-stage horizon. Vector $u_{k_t} \in R^m$ represents the control variables, and vector $x_{k_t} \in R^n$ represents time-independent variables, such as voltages, phase angles and frequency. The last set of inequality constraints guarantees that control variables do not change by more than a maximum acceptable amount between two consecutive time steps. This form of control in which the control action for the next time step is obtained by solving an online finite horizon open-loop optimal control problem, using the current state of the plant as the initial state, is known as Model Predictive Control (MPC) or Receding Horizon Control (RHC) [16].

Different levels of detail can be used for the microgrid system model, depending on the desired functionalities of the EMS and characteristics of the microgrid. In this paper, a novel three-phase dispatch model of the microgrid is developed, which is able to simulate typical unbalanced conditions of low- and medium-voltage systems and their effects on voltages and loading of both real and reactive power in each phase. This model is based on rectangular coordinates for phasor representation, and series elements (e.g., transmission/distribution lines, transformers) are represented using three-phase ABCD parameter matrices [15], [17]. The definitions of all indices, parameters and variables used in the equations below are presented in the Nomenclature section. For simplicity, the time-step index k_t has been omitted in equations that relate variables at a single time-step; such equations apply to all time steps.

A. Lines, Transformers, and Loads

Voltages and currents at sending and receiving ends are related through the following rectangular equations:

$$\begin{bmatrix} \overline{V}_{l,s} \\ \overline{I}_{l,s} \end{bmatrix} = \begin{bmatrix} A & B \\ C & D \end{bmatrix} \begin{bmatrix} \overline{V}_{l,r} \\ \overline{I}_{l,r} \end{bmatrix} \quad \forall l \tag{2}$$

where the calculation of entries of the ABCD matrices for transmission lines and transformers with different winding connections is described in [17]. Loads are modelled as a mix of constant power and constant impedance components, per phase. For constant-power loads, the relation between phase voltages and currents is described by:

$$V_{p,L} I^*_{p,L} = P_{p,L} + jQ_{p,L} \quad \forall p, \forall L \tag{3}$$

whereas constant-impedance loads are described by:

$$V_{p,L} = Z_{p,L} I_{p,L} \quad \forall p, \forall L \tag{4}$$

Phase-to-phase loads can be modelled using modified versions of (3) and (4), relating line-to-line voltages and currents. Then, these line-to-line quantities can be converted to line-to-neutral quantities using the following relationships:

$$\begin{bmatrix} V_{ab} \\ V_{bc} \\ V_{ca} \end{bmatrix} = \begin{bmatrix} 1 & -1 & 0 \\ 0 & 1 & -1 \\ -1 & 0 & 1 \end{bmatrix} \begin{bmatrix} V_a \\ V_b \\ V_c \end{bmatrix} \tag{5}$$

$$\begin{bmatrix} I_a \\ I_b \\ I_c \end{bmatrix} = \begin{bmatrix} 1 & -1 & 0 \\ 0 & 1 & -1 \\ -1 & 0 & 1 \end{bmatrix} \begin{bmatrix} I_{ab} \\ I_{bc} \\ I_{ca} \end{bmatrix} \tag{6}$$

Kirchhoff's current law at each node and phase is enforced as follows:

$$\sum_{l} I_{p,l,r_n} + \sum_{g} I_{p,g_n} = \sum_{l} I_{p,l,s_n} + \sum_{L} I_{p,L_n} \quad \forall p, \forall n \tag{7}$$

Whereas the following equation guarantees that voltages of elements connected to the same node are equal, for each phase:

$$V_{p,l,s_n} = V_{p,l,r_n} = V_{p,L_n} = V_{p,g_n} = V_{p,n} \quad \forall p, \forall n \tag{8}$$

B. Generators

Directly-connected synchronous generators are modelled as a special case of series element, as follows:

$$\begin{bmatrix} \overline{E}_g \\ \overline{I}_g \end{bmatrix} = \begin{bmatrix} \mathbf{I} & Z_{g,abc} \\ \mathbf{0} & \mathbf{I} \end{bmatrix} \begin{bmatrix} \overline{V}_g \\ \overline{I}_g \end{bmatrix} \quad \forall g \in G_s \tag{9}$$

where the per-phase impedance matrix of the machine can be estimated from the sequence impedances of the generator [18]. For simplicity, generator saliency and internal resistances are neglected in the model. With this, the positive

sequence reactance of the machine is $x_{pos,g} = x_{d,g}$. Negative- and zero-sequence reactances of the synchronous generator can be obtained from the unsaturated direct- and quadrature-axis sub-trasient reactances, as [19]: $x_{neg,g} = (x''_{d,g} + x''_{q,g})/2$, $x_{0,g} = x_{neg,g}/4 + 3x_{gnd,g}$.

The internal synchronous machine voltage is of positive sequence, which is represented by:

$$E_{a,g} + E_{b,g} + E_{c,g} = 0 \tag{10}$$

$$|E_{a,g}| = |E_{b,g}| = |E_{c,g}| \tag{11}$$

Inverter-interfaced DERs, such as high-speed microturbines, batteries, fuel cells, electrolyzers and type-4 wind turbines, feature a more flexible operation and are modelled as independent voltage sources per-phase, with current limits as follows:

$$I_{a,g} + I_{b,g} + I_{c,g} = 0 \tag{12}$$

$$|I_{a,g} + I_{b,g} + I_{c,g}| \leq I^{max}_{n,g} \tag{13}$$

Equation (12) is required for the case of 3-wire Voltage Source Converters (VSCs), whereas equation (13) will limit the maximum neutral current in the case of 4-wire VSCs. Different control strategies of VSC-interfaced DERs may impose additional constraints, such as balanced output currents, or balanced output voltages.

Directly-connected induction generators are also modelled as a special case of series elements, interfacing the machine terminals with the resistance representing the mechanical power input. Based on the sequence frame model of the induction machine [17], it is possible to relate sequence quantities of the machine's rotor and stator for the positive and negative sequences, as follows:

$$\begin{bmatrix} V_{x,st,g_i} \\ I_{x,st,g_i} \end{bmatrix} = \begin{bmatrix} a_{seq} & b_{seq} \\ c_{seq} & d_{seq} \end{bmatrix} \begin{bmatrix} V_{x,rt,g_i} \\ I_{x,rt,g_i} \end{bmatrix}, \quad x \in \{pos, neg\}, \forall g_i \tag{14}$$

where:

$$\begin{bmatrix} a_{seq} & b_{seq} \\ c_{seq} & d_{seq} \end{bmatrix} = \begin{bmatrix} 1 + \dfrac{r_s + jx_s}{jx_m} & r_s + r'_r + j(x_s + x'_r) + \dfrac{(r_s + jx_s)(r'_r + jx'_r)}{jx_m} \\ \dfrac{1}{jx_m} & 1 + \dfrac{r'_r + jx'_r}{jx_m} \end{bmatrix}$$

Being a 3-wire element, the induction machine's zero sequence circuit is an open circuit; however, the series element modelling the induction generator can be assumed to be a short circuit for zero sequence, resulting in:

$$\begin{bmatrix} V_{0,st,g_i} \\ I_{0,st,g_i} \end{bmatrix} = \begin{bmatrix} 1 & 0 \\ 0 & 1 \end{bmatrix} \begin{bmatrix} V_{0,rt,g_i} \\ I_{0,rt,g_i} \end{bmatrix} \tag{15}$$

Therefore, sequence quantities at stator terminals and rotor of the induction machine are related through:

$$\begin{bmatrix} \overline{V}_{seq,st,g_i} \\ \overline{I}_{seq,st,g_i} \end{bmatrix} = \begin{bmatrix} A_{seq} & B_{seq} \\ C_{seq} & D_{seq} \end{bmatrix} \begin{bmatrix} \overline{V}_{seq,rt,g_i} \\ \overline{I}_{seq,rt,g_i} \end{bmatrix} \tag{16}$$

where the ABCD parameter matrix of the induction generator, in the sequence frame, is defined as follows:

$$A_{seq} = \begin{bmatrix} 1 & 0 & 0 \\ 0 & a_{seq} & 0 \\ 0 & 0 & a_{seq} \end{bmatrix} B_{seq} = \begin{bmatrix} 0 & 0 & 0 \\ 0 & b_{seq} & 0 \\ 0 & 0 & b_{seq} \end{bmatrix}$$

$$C_{seq} = \begin{bmatrix} 0 & 0 & 0 \\ 0 & c_{seq} & 0 \\ 0 & 0 & c_{seq} \end{bmatrix} D_{seq} = \begin{bmatrix} 1 & 0 & 0 \\ 0 & d_{seq} & 0 \\ 0 & 0 & d_{seq} \end{bmatrix}$$

This equation can then be expressed in the natural *abc* frame by applying a standard sequence-to-phase transformation, yielding:

$$\begin{bmatrix} \overline{V}_{g_i} \\ \overline{I}_{g_i} \end{bmatrix} = \begin{bmatrix} \overline{V}_{st,g_i} \\ \overline{I}_{st,g_i} \end{bmatrix} = \begin{bmatrix} A_{g_i} & B_{g_i} \\ C_{g_i} & D_{g_i} \end{bmatrix} \begin{bmatrix} \overline{V}_{rt,g_i} \\ \overline{I}_{rt,g_i} \end{bmatrix} \quad \forall g_i \tag{17}$$

The induction generator model can be completed by describing the relation between voltages across and currents through the equivalent internal resistances of the machine by:

$$\left[\overline{I}_{rt,g_i}\right] = \frac{1}{3}\left[\left(\frac{\delta}{r_r}\right)\widetilde{\mathbf{A}} - \left(\frac{2}{r_r}\right)\widetilde{\mathbf{A}}^T\right]\left[\overline{V}_{rt,g_i}\right] \quad \forall g_i \tag{18}$$

where,

$$\widetilde{\mathbf{A}} = \begin{bmatrix} 1 & a & a^2 \\ a^2 & 1 & a \\ a & a^2 & 1 \end{bmatrix}, \quad a = 1\angle 120^\circ, \qquad \delta = \frac{s}{1-s}$$

The power generated by DERs, and their terminal currents and voltages, are related by the following complex equation:

$$P_{p,g} + jQ_{p,g} = V_{p,g} I^*_{p,g} \tag{19}$$

The total power generated by a Distributed Generator (DG) is then calculated with:

$$P_{source,g} = P_{loss,g} + \sum_p P_{p,g} \tag{20}$$

where output power losses are modelled as a function of the output current, using a quadratic term (resistive losses) plus a constant loss factor when the DG is dispatched, as follows:

$$P_{loss,g} = \begin{cases} 0 & \text{not-interfaced} \\ K_{loss,g} w_g + \sum_p |I_{p,g}|^2 r_{loss,g} & \text{VSC-interfaced} \end{cases} \tag{21}$$

Each DG's output power is limited by its maximum and minimum permitted values when turned on, or forced to zero otherwise. Thus:

$$P_{source,g} \leq P^{max}_g w_g \quad \forall g \tag{22}$$

$$P_{source,g} \geq P^{min}_g w_g \quad \forall g \tag{23}$$

The maximum power output P^{max}_g of non-dispatchable sources (e.g., wind, solar) is fixed to their forecasted values (maximum available power).

C. Energy Storage

In order to capture charging and discharging cycles of battery–ESS separately, two positive variables, $P^{out}_{g_b}$ and $P^{in}_{g_b}$, are created as follows:

$$P_{g_b} = P^{out}_{g_b} - P^{in}_{g_b} \quad \forall g_b \tag{24}$$

Hence, using a simplified book-keeping model for the State-of-charge (SOC) [20], battery-ESS balance constraints are:

$$SOC_{g_b,k_t+1} = SOC_{g_b,k_t} + \left(P^{in}_{g_b,k_t}\eta^{in}_{g_b} - \frac{P^{out}_{g_b,k_t}}{\eta^{out}_{g_b}} \right) \Delta t_{k_t} \quad \forall g_b, \forall k_t \tag{25}$$

$$SOC_{g_b,k_t} \leq SOC^{max}_{g_b} \quad \forall g_b, \forall k_t \tag{26}$$

$$SOC_{g_b,k_t} \geq SOC^{min}_{g_b} \quad \forall g_b, \forall k_t \tag{27}$$

Although equations (24)-(27) do not enforce that only one of the variables can be non-zero at a time, this will always be the case in an optimal solution of the proposed energy management problem. For example, if both $P^{in}_{g_b,k_t}$ and $P^{out}_{g_b,k_t}$ were different from zero, with $\overline{P^{in}_{g_b,k_t}} > P^{out}_{g_b,k_t}$, there would exist another combination of $\overline{P^{in}_{g_b,k_t}}$ and $\overline{P^{out}_{g_b,k_t}}$ such that $\overline{P^{in}_{g_b,k_t}} - \overline{P^{out}_{g_b,k_t}} = P^{in}_{g_b,k_t} - P^{out}_{g_b,k_t}$, with $\overline{P^{out}_{g_b,k_t}} = 0$, that produces the same power input of the battery-ESS with lower ESS losses (cheaper solution).

Hydrogen storage SOC balance constraints, at each hydrogen tank, are:

$$SOC_{H_{tank},k_t+1} = SOC_{H_{tank},k_t} + \left(\frac{1}{1+l_c} \frac{\sum_{el} P^{H_{tank}}_{el,k_t}\eta_{el}}{HHV} - \frac{\sum_{fc} P^{H_{tank}}_{fc,k_t}}{HHV\eta_{fc}} \right) \Delta t_{k_t} \quad \forall H_{tank}, \forall k_t \tag{28}$$

$$SOC_{H_{tank},k_t} \leq SOC^{max}_{H_{tank}} \quad \forall H_{tank}, \forall k_t \tag{29}$$

$$SOC_{H_{tank},k_t} \geq SOC^{min}_{H_{tank}} \quad \forall H_{tank}, \forall k_t \tag{30}$$

where $P^{H_{tank}}_{el,k_t}$ and $P^{H_{tank}}_{fc,k_t}$ are the input power of the electrolizers connected to H_{tank} at time k_t, and the output power of the fuel-cells connected to H_{tank} at time k_t, respectively.

D. Operational Constraints

The following logic constraints are necessary at each time-step to properly represent unit commitment decisions, and ensure that each DG is not turned-on and -off simultaneously:

$$u_{g,k_t} - v_{g,k_t} = w_{g,k_t} - w_{g,k_t-1} \quad \forall g, \forall k_t \tag{31}$$

$$u_{g,k_t} + v_{g,k_t} \leq 1 \quad \forall g, \forall k_t \tag{32}$$

Minimum-up and minimum-down time limits are also considered in this model, and are modelled as follows [21]:

$$\left[\sum_{\widehat{k_t}:\ t_{\widehat{k_t}} = t_{k_t} - M_{up,g}}^{k_t-1} w_{g,\widehat{k_t}} \Delta t_{\widehat{k_t}} \right] - M_{up,g}\, v_{g,k_t} \geq 0 \quad \forall g, \forall k_t \tag{33}$$

$$M_{dn,g}\,(1 - u_{g,k_t}) - \left[\sum_{\widehat{k_t}:\ t_{\widehat{k_t}} = t_{k_t} - M_{dn,g}}^{k_t-1} w_{g,\widehat{k_t}} \Delta t_{\widehat{k_t}} \right] \geq 0 \quad \forall g, \forall k_t \tag{34}$$

Equation (33) guarantees that, once turned-on, a particular DG g remains dispatched for at least $M_{up,g}$ hours. Similarly, (34) enforces minimum-down time restrictions.

The following constraints ensure DGs do not exceed their ramp-up and ramp-down limits:

$$P_{source,g,k_t+1} - P_{source,g,k_t} - u_{g,k_t+1}P^{max}_g \leq R_{up,g}\Delta t_{kt} \quad \forall g, \forall k_t \tag{35}$$

$$P_{source,g,k_t} - P_{source,g,k_t+1} - v_{g,k_t+1}P^{max}_g \leq R_{dn,g}\Delta t_{kt} \quad \forall g, \forall k_t \tag{36}$$

The objective function considers both DGs' heat-rates and costs associated with start-up and shut-down operations as follows:

$$z = \sum_{g,k_t} \left[\left(a_g P^2_{source,g,k_t} + b_g P_{source,g,k_t} + c_g w_{g,k_t} \right) \Delta t_{k_t} + C_{sup,g} u_{g,k_t} + C_{sdn,g} v_{g,k_t} \right] \tag{37}$$

where DGs driven by renewable sources and ESSs are assumed to be zero cost.

Finally, the following reserve constraint ensures that enough generation is committed at each time-step to compensate for sudden load/generation variations and/or account for contingencies:

$$\sum_{g_d} w_{g_d} \left[P^{max}_{g_d} - P_{g_d} \right] = R_{sv} \sum_{g} P_g \tag{38}$$

The energy management problem of a microgrid is defined by the minimization of the total cost z in (37), subject to constraints (2)-(13) and (17)-(38). This model is a Mixed-Integer Nonlinear Programming (MINLP) problem.

III. EMS Architecture

The microgrid's EMS should be able to optimally accommodate load variations without interfering with faster control mechanisms (primary control) [7]. Additionally, for the new dispatch commands to be meaningful, new information regarding future load and/or availability of renewable energy resources should be available from forecasting systems in place. These conditions require the EMS's update rate to be in the order of several seconds to few minutes.

MINLP problems, such as the one described in the previous section, are generally very hard to solve, and commercially available MINLP solvers are not able to find solutions in reasonable computational times, even for small-sized systems. In fact, three different MINLP solvers (BARON, KNITRO and BONMIN) were unable to obtain a solution of the complete MINLP formulation after several hours of calculation in GAMS [22]. Meta-heuristic methods have also been used to optimize this type of models; however, if not properly customized for the specific problem, they also perform poorly. Therefore, an MINLP problem formulation is not suitable for

microgrid EMS applications, and thus a decomposition of the original MINLP problem into a MILP and a Nonlinear Programming (NLP) problem is proposed here, and is shown in Fig. 2. With this approach, solutions can be obtained in the desired time-spans as discussed next.

A. Problem Decomposition

The MILP problem corresponds to the Unit Commitment (UC) problem of the single-node model of the microgrid. This relaxation considers equations (22)-(36) and (38), together with a piece-wise linear approximation of (37) [9]; depending on the size of diesel generators, a suitable linear approximation can be obtained using 1 or 2 linear segments, specially when considering the reduced operating range used to avoid carbon build-up [23]. The power flow equations (2)-(21) are replaced by a simple linear, real power, demand-supply balance equation. On the other hand, the NLP problem corresponds to a three-phase Optimal Power Flow (OPF) of the microgrid, taking the unit commitment decision variables as fixed parameters. Thus, the NLP problem comprises equations (2)-(30) and (35)-(38).

These two problems are solved sequentially. The MILP problem yields the UC decision variables (binary variables) at each time-step for the entire optimization horizon. Once this binary variables have been determined by the MILP problem, the actual dispatch strategy is re-calculated with a higher level of detail using the NLP relaxation. This refined dispatch is then implemented as reference values for the primary level control system of the microgrid, as depicted in Fig. 2.

In heavily-loaded systems, it is possible that the solution of the unit commitment variables obtained by the linear relaxation cannot be implemented in the microgrid because of insufficient reactive power resources. This condition would lead to the infeasibility of the NLP problem, and therefore malfunctioning of the EMS. To correct this issue, an additional positive variable Q^{aux}_{g,k_t} is introduced in the model. This is a positive, balanced, reactive power injection of generator g at instant k_t, which is not subject to unit commitment constraints and is penalised strongly in the objective function. If after the NLP problem is solved, there exist non-zero Q^{aux}_{g,k_t}, a feedback signal is sent to the MILP problem to increase the available generation at the corresponding time-steps. This mechanism repeats itself until all Q^{aux}_{g,k_t} in the NLP solution are below a pre-specified threshold.

It is possible that, after receiving the feedback signal from the NLP problem, the only possibility is to turn on a DG that has been recently turned off, which may render the MILP problem infeasible due of minimum-down time constraints. Although small fossil-fuel based generators are quite flexible in terms of turn-on and -off operations, it is desirable to limit them due to increased cost and frequency of maintenance. Hence, minimum-down time and minimum-up time constraints are not necessarily technical limits of the devices, but rather desired operational conditions. In order to account for this condition and avoid infeasibility of the MILP problem, a high-cost emergency turn-on and turn-off operation is allowed by introducing auxiliary variables u^{emer}_{g,k_t} and v^{emer}_{g,k_t}. Therefore, minimum-up and minimum-down time constraints are modified as follows:

$$\left[\sum_{\widehat{k_t}:\ t_{\widehat{k_t}}=t_{k_t}-M_{up,g}}^{k_t-1} w_{g,\widehat{k_t}}\Delta t_{\widehat{k_t}}\right] - M_{up,g}\left(v_{g,k_t}-v^{emer}_{g,k_t}\right)\geq 0 \quad \forall g,\forall k_t \tag{39}$$

$$M_{dn,g}\left(1-\left(u_{g,k_t}-u^{emer}_{g,k_t}\right)\right) - \left[\sum_{\widehat{k_t}:\ t_{\widehat{k_t}}=t_{k_t}-M_{dn,g}}^{k_t-1} w_{g,\widehat{k_t}}\Delta t_{\widehat{k_t}}\right]\geq 0 \quad \forall g,\forall k_t \tag{40}$$

These two equations require a re-formulation of the total cost of operation defined in (37) as follows:

$$\begin{aligned} z=\sum_{g,k_t}\big[&\left(a_g P^2_{source,g,k_t}+b_g P_{source,g,k_t}+c_g w_{g,k_t}\right)\Delta t_{k_t} \\ &+C_{sup,g}u_{g,k_t}+C_{sdn,g}v_{g,k_t}+K_{Q^{aux}}Q^{aux}_{g,k_t}+ \\ &K_{emer}(u^{emer}_{g,k_t}+v^{emer}_{g,k_t})\big] \end{aligned} \tag{41}$$

Where weighting factor $K_{Q^{aux}}$ must be high enough to guarantee that all reactive power resources from the available DGs are utilized first, and Q^{aux}_{g,k_t} is used only as the last resort. Similarly, a high value of K_{emer} guarantees that emergency turn-on and turn-off operations are only used to avoid infeasibility.

B. MPC Implementation

As discussed previously in this section, dispatch commands should be re-calculated by the EMS with update rates in the order of several seconds to few minutes. In this work, an update rate of 5 minutes is chosen, which is consistent with the fastest available wind/solar power forecasting systems and suitable for capturing typical load fluctuations. Thus, every 5 minutes the EMS action is triggered, and the energy management problem is solved according to the aforementioned procedure.

Unit commitment decision variables typically follow slower dynamics as compared to dispatch commands. While optimal dispatch commands are expected to change with slight changes in the load, the optimal unit commitment decisions respond to longer-term trends in load variations. Thus, it is not necessary to obtain a new solution for the MILP problem with the same frequency of that of the NLP problem. Despite the above fact, the MILP problem is typically much easier and faster to solve, and therefore there is no significant advantage in solving the MILP problem at a slower rate in terms of computational effort. The MILP problem requires a longer optimization horizon as compared to the NLP problem in order to capture slower load patterns that affect unit commitment decisions. Furthermore, it is not computationally efficient to calculate unbalanced OPFs over extended horizons, considering that future dispatches are very likely to change as forecasts are

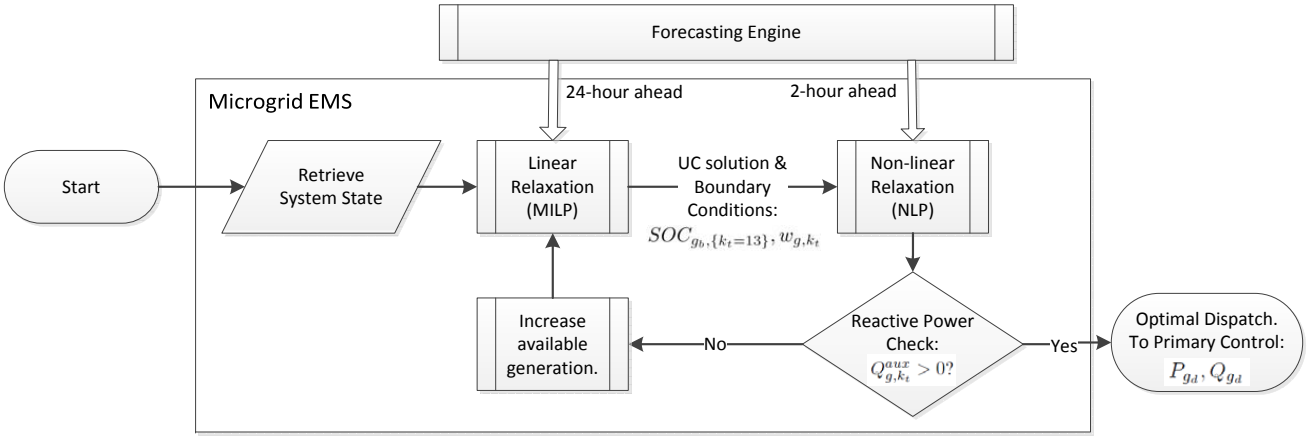

Fig. 2: EMS problem decomposition.

updated. In this work, a horizon of 24 hours is used for the MILP problem, while a 2-hours horizon is selected for the NLP problem. Hence, the MILP problem is able to capture daily load and renewable generation patterns, and provide boundary conditions for the SOC of ESSs in the NLP problem. The NLP problem then calculates detailed dispatch strategies, and is able to detect power flow problems in a shorter term.

C. Time Resolution and Forecasting System

The proposed EMS uses a moving horizon of 24 hours, but it does not consider a homogeneous time resolution over this time span. While the first few minutes can be forecasted with high accuracy and resolution, the resolution decreases as the forecasting horizon is extended. This characteristic responds to limitations of existing forecasting systems; however, it is also a desirable trait, as more detailed information is required for operation scenarios in the near future (more certain scenarios) than for less certain future scenarios. Particularly, in the case of the MILP problem, using a fixed 5-minutes resolution over the entire horizon will result in a total of 286 time-steps to cover the 24-hour look-ahead window, which is quite impractical considering that the calculation is performed again in the next 5 minutes. Hence, a variable forecasting resolutions is used here to attain a higher level of detail in first next few hours, and lower detail (or resolution) afterwards. This way, the number of time steps in the look-ahead window is reduced, and different types of forecast can be used (e.g., time-series, neural networks, phenomenological models) depending on the corresponding look-ahead window [24]. Thus, 4 different consecutive time resolutions are used in the proposed EMS, as follows (see Fig. 3):

- 6 time-steps of 5 minutes (MILP & NLP),
- 6 time-steps of 15 minutes (MILP & NLP),
- 6 time-steps of 30 minutes (MILP), and
- 19 time-steps of 60 minutes (MILP).

The effect of forecasting system accuracy is not studied in this work; however, the accuracy of the predictions will have an impact on the performance of the proposed EMS, affecting the optimality of the solutions (inherently suboptimal) due to imperfect information. Nevertheless, given the fast update rate of the proposed EMS (5 minutes), the implemented solution is not expected to deviate too much from the forecasted value (5-minutes ahead). It is important to note that the EMS is a supervisory control, and the actual power output of DG units will be determined by local primary controllers (droop controllers) which will adjust the dispatch settings produced by the EMS based on frequency and voltage set points.

IV. Results

A. Test System

The designed centralized EMS for isolated microgrids is tested on a CIGRE medium voltage network presented in [25], which is based on the European medium-voltage distribution network benchmark. A single-line diagram of the 16-bus 12.47 kV test system is shown in Fig. 4, based on the diagram provided in [25]. In this modified test system, a connection to the main grid has been replaced by a bus with 3 diesel units, with a combined capacity of 4,700 kW. The system features a total installed capacity of 8,760 kW, considering battery-ESS, fuel-cells, and intermittent renewable energy sources. The loads have been divided into 2 categories, residential and commercial, with different daily load profiles and a combined peak load of approximately 4,800 kW. Nominal ratings of DGs are shown in Table I. Typical values are assumed for technical parameters and heat-rates of DGs (e.g. [26], [27]). Additional details about the test system are provided in the Appendix.

Many medium-voltage networks operate under unbalanced conditions due to single-phase feeder connections, or uneven distribution of loads. For example, autonomous grids supplying remote communities in Northern Canada present seasonal phase imbalance due to different distribution of loads in summer and winter times. For this reason, loads in the test system have been considered unevenly distributed among the 3 phases, with phase-a feeding 30.2%, phase-b 35.7%, and phase-c a 34.2% of the total load. Single-phase feeders have been represented as lumped single-phase passive loads. Residential loads are assumed to be composed of 80% constant impedance load, and 20% constant power load, whereas

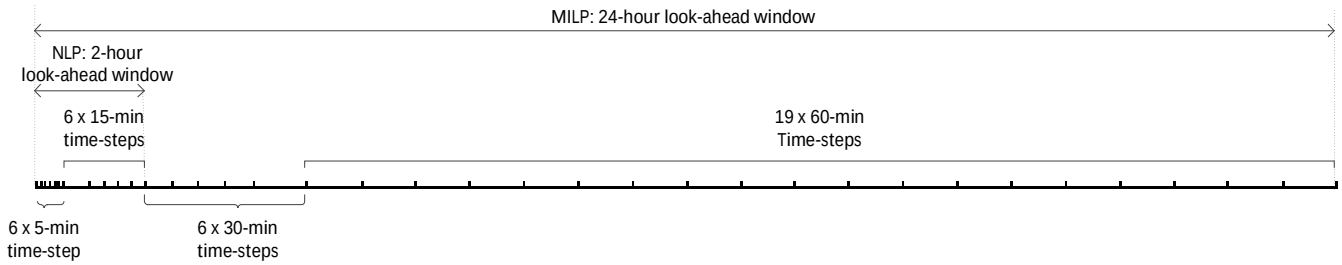

Fig. 3: EMS horizon variable time-steps.

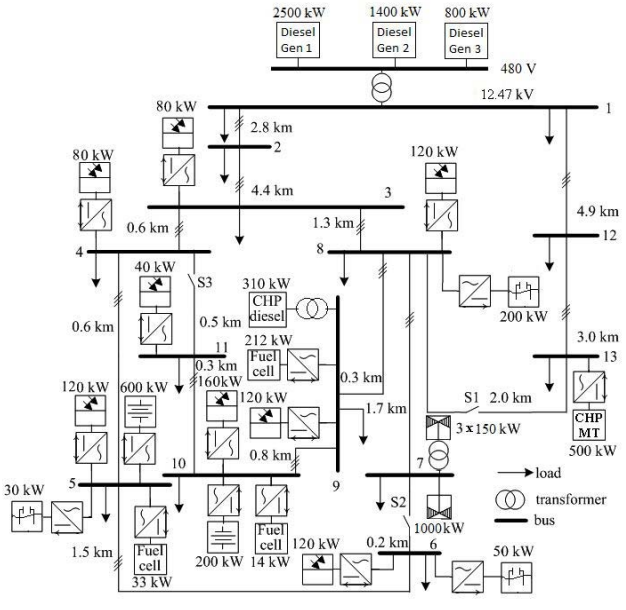

Fig. 4: Modified CIGRE microgrid benchmark.

TABLE I: MICROGRID TEST SYSTEM DERS RATINGS

No.	Node	DER type	P_{max} $[kW]$
1	14	Diesel Generator	800
2	15	CHP diesel	310
3	14	Diesel Generator	1400
4	14	Diesel Generator	2500
5	3	Photovoltaic	80
6	4	Photovoltaic	80
7	5	Photovoltaic	120
8	5	Battery	600
9	5	Residential fuel cell	33
10	5	Electrolyzer	30
11	6	Photovoltaic	120
12	6	Electrolyzer	50
13	8	Photovoltaic	120
14	8	Electrolyzer	200
15	9	Photovoltaic	120
16	9	CHP fuel cell	212
17	10	Photovoltaic	160
18	10	Battery	200
19	10	Residential fuel cell	14
20	11	Photovoltaic	40
21	13	CHP Microturbine	500
22	7	Wind turbine (inverter-interfaced)	1000
23	16	Wind turbine (SCIG)	150
24	16	Wind turbine (SCIG)	150
25	16	Wind turbine (SCIG)	150

commercial loads are composed of 50% constant impedance load and 50% constant power load. Residential load, wind power and solar power forecasts are obtained from real data from a real forecasting systems used in a rural microgrid in Huatacondo, Chile [9].

The EMS is assumed to have full autonomous control over the dispatch of every DG in the microgrid, and is provided with updated load and renewable generation forecasts every 5 minutes.

B. Simulation Results

The performance of the EMS is tested for 24 hours of operation, with dispatch updates every 5 minutes. The model is coded in the high-level optimization modelling language GAMS [22], and MILP and NLP problems are solved using CPLEX [28] and COIN-IPOPT [29] solvers, respectively. In addition to equations presented in Section III and IV, per-phase output current limits and voltage limits are also included in the model.

For comparison purposes, the optimal dispatch is calculated for two cases: the detailed unbalanced microgrid model and the balanced microgrid model approximation. The balanced microgrid approximation, where the loads are assumed to be evenly shared among the phases, represents a less critical scenario in terms of system losses, voltage drops and reactive power requirements as compared to the exact unbalanced network model. This can be illustrated in an extreme example where the same power is distributed evenly among the phases, versus the case where the load is concentrated in only one of the phases; in this case, it is clear that the unbalanced case will yield higher system losses (active and reactive power) and larger voltage drops.

The total simulation time is 8,392s for 286 iterations of the EMS, thus yielding an average computational time of approximately 30s per iteration, which is within the desired 5-minutes dispatch window, making it suitable for real-time applications. Results of the optimal dispatch are shown in Fig. 5 using a stacked-area plot. For simplicity, only the main dispatchable units have been included in Fig. 5, namely, diesel units, microturbine, and battery-ESSs. The optimal dispatch of battery-ESSs has been plotted in a way to properly show charging and discharging cycles; hence, negative areas in the figure correspond to charging cycles of the batteries. The total load profiles for both balanced and unbalanced models are also included in Fig. 5. For completeness, Fig. 6 shows the power

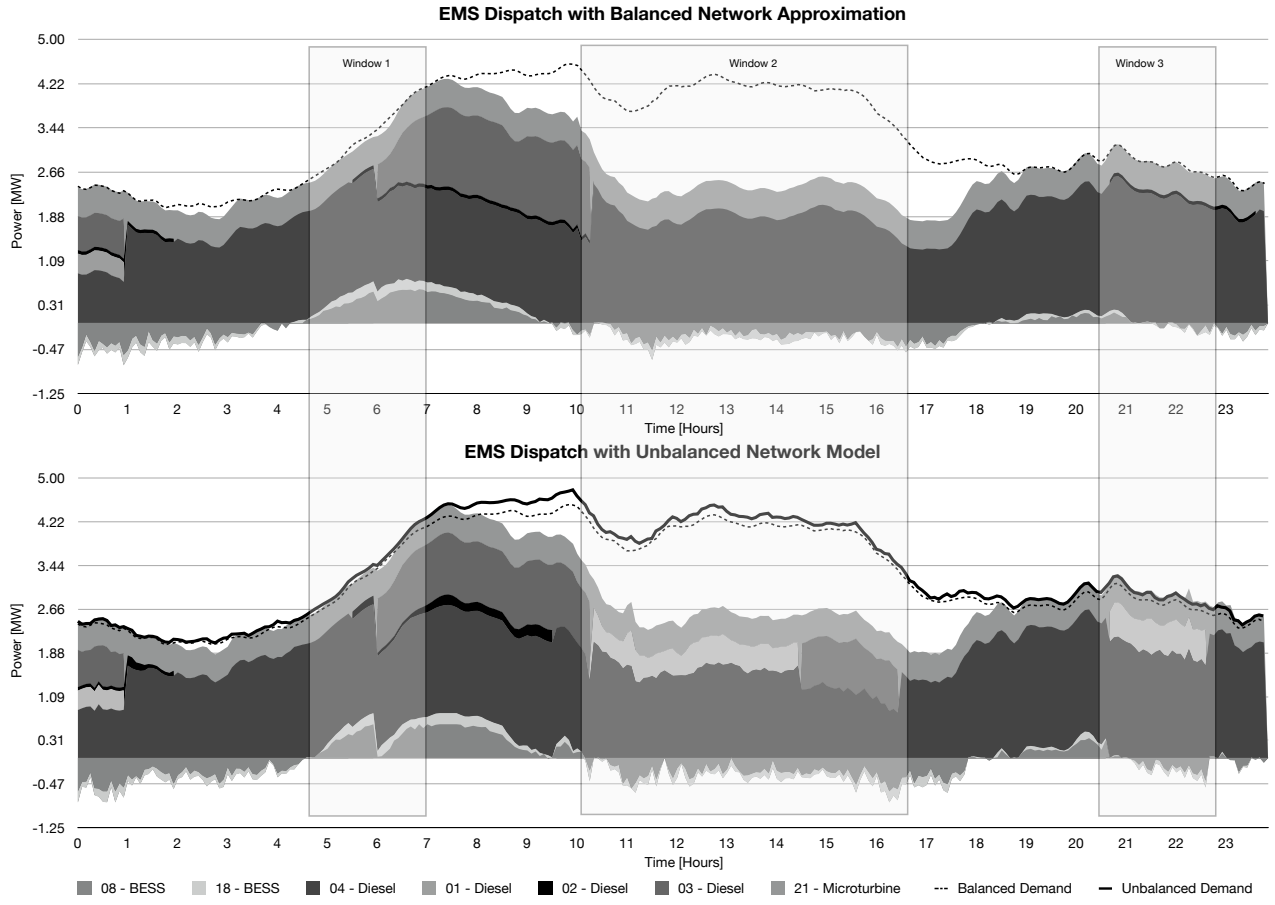

Fig. 5: Optimal dispatch obtained by the EMS for balanced and unbalanced studies.

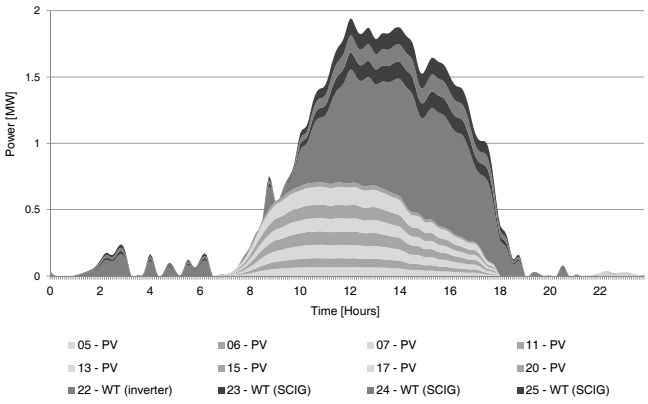

Fig. 6: Renewable generation power injections.

from renewable DGs, which fills the white gaps between the main dispatchable units and the total load in Fig. 5, for both balanced and unbalanced cases. Powers from the rest of the units, namely, fuel-cells and electrolizers, are not shown, since these do not participate significantly in the dispatch for this particular test system due to their low efficiencies. Note in Fig. 5 that both cases have some similarities on the dispatch over the 24-hour window; however, differences can be found in the actual dispatch of the units, and more importantly, in the UC decisions. In particular, 3 time-windows of interest can be identified in the figure:

1) Window 1: The same units are committed in both cases for this window; however, significant differences in the dispatch commands can be observed for Unit-02 (diesel), Unit-08 and Unit-18 (battery-ESSs). After Unit-03 (diesel) is turned-on around hour 6, battery-ESSs units show a significantly higher dispatch in the balanced approximation case as compared to the unbalanced model case. This can be attributed to an underestimation of future load requirements in the balanced approximation, which translates into more power available for present use, and less reserves required for future operation.

2) Window 2: After Unit-03 is turned-off (near hour 10), Unit-04 increases its dispatch to supply the load in the balanced approximation. However, the unbalanced model detects reactive power problems that were overlooked by the balanced approximation when Unit-03 is turned-off. Unit-03 cannot be turned back on immediately due to minimum-down time and minimum power output constraints; instead, Unit-01 is turned-on to supply the deficit. After Unit-01 is turned-on, the MILP problem generates turn-off signals for this machine in the following time-steps, since this formulation does not include reactive power problems; however, Unit-01 is prevented from turning-off by the OPF NLP solution. After 4 hours, Unit-01

is replaced by the more economical Unit-03.

3) Window 3: In this window, the commitment of Unit-02 is considered enough by the balanced approximation, whereas the unbalanced model requires the operation of the bigger Unit-01 due to reactive power requirements. Furthermore, it can be observed that battery-ESSs (Unit-08 and Unit-18) are dispatched to absorb more power in the unbalanced model due to the commitment of Unit-01.

The total load is underestimated by a balanced approximation of an unbalanced microgrid for 2 main reasons:

- The same load, supplied in an unbalanced configuration, will produce higher system losses as compared to a balanced configuration, as previously explained.
- The power absorbed by impedance loads is voltage-dependent; therefore, in an unbalanced network, higher voltages in one of the phases will lead to higher power.

It can be observed in Fig. 5 that the underestimation of the total load by the balanced approximation is more critical during peak-load hours (between hours 6 and 16). Thus, differences in the dispatch commands obtained with balanced and unbalanced models are more significant in heavily-loaded systems, while it may go unnoticed in lightly-loaded microgrids. Hence, dispatch commands produced by EMSs based on balanced approximations of unbalanced microgrids may lead to underestimation of the active and reactive power requirements, or infeasible dispatch solutions.

Table II shows a summary of the simulation results. A total of 80 warning feedback signals of reactive power deficits are generated in the detailed unbalanced model, while these problems are not detected by the balanced approximation. Peak load is under-estimated by 5% by the balanced approximation, yielding a 7.05% under-estimation of the cost.

TABLE II: SUMMARY OF SIMULATION RESULTS

	Unbalanced Model	Balanced Model
No. of iterations with $u^{emer}_{g,k_t} > 0$	1	0
No. of iterations with $v^{emer}_{g,k_t} > 0$	6	24
No. of iterations with $Q^{aux}_{g,k_t} > 0$	80	0
Peak load	4.81 MW	4.57 MW
Total cost of dispatch (24 hours)	$16,405.10	$15,249.10

V. CONCLUSIONS

The paper presented a detailed three-phase EMS for isolated microgrids. System variables were represented as phasors in the rectangular form, and the natural *abc* frame was used. Transmission lines and transformers were represented using ABCD parameter matrices, and three different types of DG models were included: synchronous generators, induction generators and inverter-interfaced sources. Loads were modelled as a combination of constant power and constant impedance components. The EMS was formulated using an MPC approach, by iteratively solving a multi-stage MINLP problem. In order to reduce computational time, the resulting MINLP problem was decomposed into two problems, an MILP problem, and an NLP problem. This decomposition is able to obtain solutions within the desired time spans where commercial MINLP solvers failed to obtain a solution, enabling the potential implementation of the EMS in real-time, autonomous operation of isolated microgrids.

The proposed EMS is able to account for the effects of system unbalance on the optimal dispatch of the microgrid, and correct potential reactive power deficits. Simulations showed that, under certain loading conditions, neglecting system unbalance can lead to deviations of the optimal dispatch strategy or the inability of the system to meet reactive power requirements. The results substantiate the need for a detailed three-phase model of the microgrid for EMS applications; however, for a more detailed analysis of the quality of the solutions, a complete, real-time model of the microgrid that includes the effects of primary controllers is required. Future work will concentrate on increasing the robustness of the proposed EMS model against uncertainties in the forecasting system by applying robust and stochastic optimization techniques.

APPENDIX
TEST SYSTEM DATA

The test system data presented in Tables IV and V was obtained from a CIGRE document to be published shortly. Table III contains additional data associated with transformers interfacing additional generators included in the particular test system used in for this work. Tables VI, VII and VIII contain technical parameters of DERs based on synchronous generators, inverter-interfaced, and squirrel-cage induction generators, respectively, obtained from multiple sources. Finally, Table IX contains data associated with operating costs of fuel-driven DGs.

TABLE III: TRANSFORMERS PARAMETERS

TF No	Node from	X [pu]	*Type*	V from [kV]	V to [kV]	S_{rated} [kVA]
1	14-1	0.05	$\Delta - Y$	0.48	12.47	5,000
2	15-9	0.05	$\Delta - Y$	0.48	12.47	500
3	16-7	0.05	$\Delta - Y$	0.48	12.47	700

TABLE IV: LINE PARAMETERS

Line No	Node from-to	R_{ph} [Ω]	X_{ph} [Ω]	B_{ph} [μS]	R_0 [Ω]	X_0 [Ω]	B_0 [μS]
1	1-2	0.208	0.518	4.596	0.421	2.160	1.884
2	2-3	0.173	0.432	3.830	0.351	1.800	1.570
3	3-4	0.106	0.264	2.336	0.214	1.098	0.958
4	4-5	0.097	0.242	2.145	0.197	1.008	0.879
5	5-6	0.266	0.665	5.898	0.541	2.772	2.418
6	6-7	0.042	0.104	0.919	0.084	0.432	0.377
7	7-8	0.289	0.721	6.396	0.586	3.006	2.622
8	8-9	0.055	0.138	1.226	0.112	0.576	0.502
9	9-10	0.133	0.333	2.949	0.270	1.386	1.209
10	10-11	0.057	0.143	1.264	0.116	0.594	0.518
11	11-4	0.085	0.212	1.877	0.172	0.882	0.769
12	3-8	0.225	0.562	4.979	0.456	2.340	2.041
13	1-12	0.846	2.112	18.729	1.716	8.802	7.677
14	12-13	0.517	1.292	11.452	1.049	5.382	4.694
15	13-8	0.346	0.864	7.660	0.702	3.600	3.140

TABLE V: LOAD PARAMETERS

Node	Apparent Power [kVA] Phase A		Phase B		Phase C		Power Factor	
	Residential	Commercial	Residential	Commercial	Residential	Commercial	Residential	Commercial/Industrial
1	344.00	80.00	172.00	180.00	200.00	180.00	0.90	0.80
2	100.00	200.00	50.00	200.00	0.00	200.00	0.95	0.85
3	0.00	80.00	200.00	80.00	50.00	80.00	0.90	0.80
4	200.00	0.00	100.00	0.00	100.00	0.00	0.90	1.00
5	200.00	50.00	172.00	200.00	0.00	50.00	0.95	0.85
6	50.00	0.00	100.00	0.00	172.00	0.00	0.95	1.00
7	0.00	100.00	100.00	100.00	0.00	100.00	0.95	0.95
8	100.00	0.00	150.00	0.00	0.00	200.00	0.90	0.90
9	100.00	0.00	150.00	0.00	100.00	0.00	0.95	1.00
10	150.00	0.00	100.00	0.00	250.00	0.00	0.90	1.00
11	50.00	150.00	50.00	150.00	0.00	150.00	0.95	0.85
12	0.00	145.00	0.00	145.00	0.00	145.00	0.95	0.85
13	0.00	90.00	0.00	90.00	172.00	90.00	0.90	0.90

TABLE VI: DIRECTLY-CONNECTED SYNCHRONOUS GENERATORS PARAMETERS

Unit No.	S_{base} [kVA]	V_{base} [kV]	P_{max} [kW]	P_{min} [kW]	x_d [pu]	x''_d [pu]	x''_q [pu]	x_0 [pu]
1	1000	0.48	800	350	3.05	0.134	0.153	0.051
2	390	0.48	310	60	3.5	0.142	0.166	0.038
3	1750	0.48	1400	600	3.05	0.134	0.153	0.051
4	3125	0.48	2500	1000	3.05	0.134	0.153	0.051

TABLE VII: INVERTER-INTERFACED DERS PARAMETERS

	DER				Inverter		
Unit No.	P_{max} [kW]	P_{min} [kW]	*Eff*$_{in}$ (ESS) [%]	*Eff*$_{out}$ (ESS) [%]	S_{max} [kVA]	*Eff*-at-P_{max} [%]	*Eff*-at-20%P_{max} [%]
5	20	0	-	-	250	91%	95%
6	20	0	-	-	250	91%	95%
7	30	0	-	-	375	91%	95%
8	600	0	95%	95%	750	91%	95%
9	33	6	-	60%	42	91%	95%
10	30	6	60%	-	38	91%	95%
11	30	0	-	-	38	91%	95%
12	50	10	60%	-	63	91%	95%
13	30	0	-	-	38	91%	95%
14	200	40	60%	-	250	91%	95%
15	30	0	-	-	38	91%	95%
16	212	50	-	60%	265	91%	95%
17	40	0	-	-	50	91%	95%
18	200	0	95%	95%	250	91%	95%
19	14	0	-	60%	18	91%	95%
20	10	0	-	-	13	91%	95%
21	500	100	-	-	625	91%	95%
22	1000	0	-	-	1250	91%	95%

TABLE VIII: DIRECTLY-CONNECTED SCIG PARAMETERS

Unit	S_{base}	V_{base}	P_{max}	P_{min}	r_s	x_s	r'_r	x'_r	x_m
No.	[kVA]	[kV]	[kW]	[kW]	[pu]	[pu]	[pu]	[pu]	[pu]
23	190	0.48	150	0	0.007	0.15	0.0072	0.15	2.95
24	190	0.48	150	0	0.007	0.15	0.0072	0.15	2.95
25	190	0.48	150	0	0.007	0.15	0.0072	0.15	2.95

TABLE IX: HEAT RATES, START-UP AND SHUT-DOWN COSTS

Unit	a	b	c	C_{Sup}	C_{Sdn}
No.	$[lt/kWh^2]$	$[lt/kWh]$	$[lt]$	$[lt]$	$[lt]$
1	0	0.2881	7.5	15	5.3
2	0	0.2876	0	7.35	1.44
3	0	0.2571	25.5	45	8.3
4	0.00001	0.224	45.5	95	15.3
	$[MBTu/kWh^2]$	$[MBTu/kWh]$	$[MBTu]$	$[MBTu]$	$[MBTu]$
21	0.0106	0.6	2	0.09	0

REFERENCES

[1] B. Lasseter, "Microgrids [distributed power generation]," in *Proc. IEEE-PES Winter Meeting, 2001*, vol. 1, Jan. 2001, pp. 146 –149 vol.1.

[2] N. Hatziargyriou, H. Asona, R. Iravani, and C. Marnay, "Microgrids," *IEEE Power Energy Mag.*, vol. 5, no. 4, pp. 78–94, Jul./Aug. 2007.

[3] "Advanced Architectures and Control Concepts for MORE MICROGRIDS: Definition of Ancillary Services and Short-Term Energy Markets," Deliverable DD4, MORE MICROGRIDS, Dec. 2009. [Online]. Available: http://www.microgrids.eu/documents/686.pdf

[4] A. L. Dimeas and N. D. Hatziargyriou, "Operation of a multiagent system for microgrid control," *IEEE Trans. Power Syst.*, vol. 20, no. 3, pp. 1447–1455, Aug. 2005.

[5] T. Logenthiran, D. Srinivasan, and D. Wong, "Multi-agent coordination for DER in microgrid," in *Proc. IEEE International Conference on Sustainable Energy Technologies, 2008*, Nov. 2008, pp. 77–82.

[6] J. Oyarzabal, J. Jimeno, J. Ruela, A. Engler, and C. Hardt, "Agent based micro grid management system," in *Proc. IEEE International Conference on Future Power Systems, 2005*, Nov. 2005, pp. 6 pp. –6.

[7] D. Olivares, C. Canizares, and M. Kazerani, "A centralized optimal energy management system for microgrids," in *Proc. IEEE PES General Meeting, 2011*, July 2011, pp. 1–6.

[8] M. Korpas and A. Holen, "Operation planning of hydrogen storage connected to wind power operating in a power market," *IEEE Trans. Energy Convers.*, vol. 21, no. 3, pp. 742 –749, Sept. 2006.

[9] R. Palma-Behnke, C. Benavides, F. Lanas, B. Severino, L. Reyes, J. Llanos, and D. Sáez, "A microgrid energy management system based on the rolling horizon strategy," *IEEE Trans. Smart Grid*, vol. 4, no. 2, pp. 996–1006, 2013.

[10] T. Logenthiran and D. Srinivasan, "Short term generation scheduling of a microgrid," in *Proc. IEEE Region 10 Conference, 2009 (TENCON'09)*, Jan. 2009, pp. 1 –6.

[11] E. Barklund, N. Pogaku, M. Prodanovic, C. Hernandez-Aramburo, and T. C. Green, "Energy management in autonomous microgrid using stability-constrained droop control of inverters," *IEEE Trans. Power Electron.*, vol. 23, no. 5, pp. 2346–2352, August 2008.

[12] R. Firestone and C. Marnay, "Energy manager design for microgrids," Consortium for Electric Reliability Technology Solutions (CERTS), Tech. Rep., 2005.

[13] M. Dolan, E. Davidson, I. Kockar, G. Ault, and S. McArthur, "Distribution power flow management utilizing an online optimal power flow technique," *IEEE Trans. Power Syst.*, vol. 27, no. 2, pp. 790–799, 2012.

[14] A. Gabash and P. Li, "Active-reactive optimal power flow in distribution networks with embedded generation and battery storage," *IEEE Trans. Power Syst.*, vol. 27, no. 4, pp. 2026–2035, 2012.

[15] S. Paudyal, C. Canizares, and K. Bhattacharya, "Optimal operation of distribution feeders in smart grids," *Industrial Electronics, IEEE Transactions on*, vol. 58, no. 10, pp. 4495–4503, 2011.

[16] R. Findeisen, "Nonlinear model predictive control: A sampled–data feedback perspective," Ph.D. dissertation, Univ. Stuttgart, 2004.

[17] W. H. Kersting, *Distribution System Modeling and Analysis, Second Edition*, 2nd ed. Bosa Roca, FL, USA: CRC Press, 2006.

[18] A. Gomez-Exposito, A. J. Conejo, and C. Canizares, Eds., *Electric Energy Systems Analysis and Operation*, 1st ed. Bosa Roca, FL, USA: CRC Press, 2009.

[19] J. Tamura, I. Takeda, M. Kimura, M. Ueno, and S. Yonaga, "A synchronous machine model for unbalanced analyses," *Elect. Eng. Jpn.*, vol. 119, pp. 46–59, 1997.

[20] H. Bergveld, "Battery Management Systems Design by Modelling," Ph.D. dissertation, Univ. Twente, 2001.

[21] J. Arroyo and A. Conejo, "Optimal response of a thermal unit to an electricity spot market," *IEEE Trans. Power Syst.*, vol. 15, no. 3, pp. 1098–1104, 2000.

[22] R. E. Rosenthal, *GAMS – A User's Guide*, GAMS Development Corporation, Washington, DC, USA, December 2012.

[23] M. Arriaga, C. Canizares, and M. Kazerani, "Renewable Energy Alternatives for Remote Communities in Northern Ontario, Canada," *Sustainable Energy, IEEE Transactions on*, vol. 4, no. 3, pp. 661–670, 2013.

[24] S. Soman, H. Zareipour, O. Malik, and P. Mandal, "A review of wind power and wind speed forecasting methods with different time horizons," in *Proc. North American Power Symposium (NAPS), 2010*, 2010, pp. 1–8.

[25] K. Rudion, A. Orths, Z. Styczynski, and K. Strunz, "Design of benchmark of medium voltage distribution network for investigation of dg integration," in *Proc. IEEE PES General Meeting, 2006*, 2006, pp. 1–6.

[26] "Continuous 1650 ekW, 2063 kVA Diesel Genset Datasheet," Caterpillar, 2012. [Online]. Available: http://www.cat.com/en_US/products/new/power-systems/electric-power-generation/diesel-generator-sets/

[27] "Prime 513 kVA Diesel Genset Model DFEJ 60 Hz Datasheet," Cummins Power Generation, 2004-2006. [Online]. Available: https://www.cumminsgeneratortechnologies.com/en/download/datasheets/displayDownloadDatasheets.do

[28] CPLEX 12, Solver Manual. [Online]. Available: http://www.gams.com/dd/docs/solvers/cplex.pdf

[29] A. Wchter and L. T. Biegler, "On the implementation of an interior-point filter line-search algorithm for large-scale nonlinear programming," *Mathematical Programming*, vol. 106, pp. 25–57, 2006. [Online]. Available: http://dx.doi.org/10.1007/s10107-004-0559-y

Daniel E. Olivares (S'11) was born in Santiago of Chile, received the B.Sc. and the Engineer degree in electrical engineering from the University of Chile, Santiago, Chile, in 2006 and 2008 respectively. He is currently working toward the Ph.D. degree in electrical and computer engineering at the University of Waterloo, Waterloo, ON, Canada. His research interests include modelling, simulation, control and optimization of power systems in the context of smart grids.

Claudio A. Cañizares (S86, M91, SM00, F07) received the electrical engineer diploma from the Escuela Politcnica Nacional (EPN), Quito, Ecuador, in 1984 and the M.S. and Ph.D. degrees electrical engineering are from the University of Wisconsin-Madison in 1988 and 1991, respectively. He has held various academic and administrative positions at the Electrical and Computer Engineering Department of the University of Waterloo, Waterloo, ON, Canada, since 1993, where he is currently a full Professor and the Associate Director of the Waterloo Institute for Sustainable Energy (WISE). He was awarded the Hydro One research chair in 2010. His research activities concentrate in the study of stability, modeling, simulation, control, and computational issues in power systems within the context of competitive electricity markets and smart grids.

Dr. Cañizares has been the recipient of various IEEE-PES Working Group awards and holds and has held several leadership appointments in IEEE-PES technical committees and subcommittees. He is Registered Professional Engineer in the province of Ontario and Fellow of the Royal Society of Canada.

Mehrdad Kazerani (S88, M96, SM02) received the B.Sc. degree from Shiraz University, Iran, the M. Eng. degree from Concordia University, Canada, and the Ph.D. degree from McGill University, Canada, in 1980, 1990, and 1995, respectively. From 1982 to 1987, he was with the Energy Ministry of Iran. He is currently a Professor at the Department of Electrical and Computer Engineering, University of Waterloo, Waterloo, ON, Canada. His research interests include power electronic circuits and systems design, power quality/active power filters, matrix converters, distributed power generation, utility interface of alternative energy sources, battery electric, hybrid electric and fuel cell vehicles, and FACTS.

Dr. Kazerani is a Registered Professional Engineer in the province of Ontario.